Phonon imaging in superconducting Pb crystals: Absence of large gap anisotropy and spin-density waves

J. D. Short,* T. L. Head,† and J. P. Wolfe
Physics Department and Materials Research Laboratory, University of Illinois at Urbana-Champaign, Urbana, Illinois 61801, USA
(Received 28 November 2007; revised manuscript received 16 July 2008; published 22 August 2008)

We show that anisotropies in the electronic structure of a superconducting metal can be probed with ballistic acoustic phonons at low temperatures. We were motivated by the possibility that Pb has narrow valleys of lowered gap, possibly caused by the spin-density wave (SDW) postulated by Overhauser and Daemen [Phys. Rev. Lett. **61**, 1885 (1988)]. Our experiments and analysis on crystals of different thickness, plus results with a phonon-frequency filter, do not support their idea of deep valleys in the superconducting gap parameter. For a spherical Fermi surface, phonon scattering would be isotropic but for the highly anisotropic Fermi surface of Pb, the scattering rate depends on the direction of the phonon wave vector, **q**. To observe this anisotropy, we perform phonon-imaging experiments on high-purity Pb crystals cooled between 1.45 and 2.1 K. At this low temperature the mean-free path of a phonon can extend to millimeter distances if its energy is less than the superconducting energy gap, $2\Delta_o$. In this regime, phonons are absorbed by thermally excited quasiparticles on the Fermi surface. Phonon images show a striking pattern of phonon absorption that becomes stronger as the temperature is raised. The anisotropy is explained by a calculation of phonon scattering on the actual Fermi surface of Pb without recourse to SDWs. The preliminary temperature dependences reported in this paper, which assumes that the quasiparticles doing the scattering are in equilibrium at the lattice temperature, are much weaker than the low-temperature form $\exp(-\Delta_o/k_BT)$ predicted by the BCS theory of superconductivity. Even accounting for the inherent scattering of phonons from isotopes in the crystal, we find a path-length dependence of phonon-absorption coefficient inconsistent with deep SDW valleys. A phonon filter experiment designed to attenuate phonons that would eject quasiparticles from such valleys clearly supports this conclusion. A resolution of the anomalous temperature and sample-length dependences, plus a measurement of the superconducting gap by phonon-imaging, is reported in the following paper.

DOI: 10.1103/PhysRevB.78.054515 PACS number(s): 74.25.Ld, 74.25.Jb, 72.10.Di, 75.30.Fv

I. INTRODUCTION

In a normal metal the mean-free-path of phonons is limited to submicrometer distances by electron-phonon scattering. In a superconductor, however, phonons with energy less than the low-temperature superconducting energy gap, $2\Delta_o$, may propagate millimeter distances as they are incapable of breaking Cooper pairs. At nonzero temperatures, phonons may scatter from *quasiparticles*, the basic electronic excitations of a superconductor, which result from thermally broken Cooper pairs.

Phonon scattering from electrons or quasiparticles depends on the electronic structure of the metal, in particular, the shape of the Fermi surface. The electronic structure of metals composed of elements with large valency is quite complicated. Crystalline Pb, with four valence electrons per unit cell, has a Fermi surface that cuts across the second and third Brillouin zones. This intricate surface has been characterized in great detail, mainly by de Haas-van Alphen experiments and subsequent theoretical analyses.[1]

The complicated Fermi surface of Pb implies a corresponding complexity in the scattering of phonons from electrons. Momentum conservation dictates that a phonon with wave vector **q** scatters an electron with wave vector $\mathbf{k}_i$ to wave vector $\mathbf{k}_f=\mathbf{k}_i+\mathbf{q}$. In the experiments to be described, the relevant acoustic phonons have energies of a few meV and wave vectors of up to 1.5×10^7 cm^{-1}. These phonon energies are three orders of magnitude less than the Fermi energy (E_F=9.7 eV in Pb) but the phonon momenta $\hbar k$ are a much more significant fraction of the Fermi momentum ($k_F=1.57\times10^8$ cm^{-1}). Thus, when an electron is scattered by absorbing a phonon, energy and momentum conservation requires that **q** must lie nearly along the Fermi surface. For a spherical Fermi surface, the phonon wave vector is nearly perpendicular to $\mathbf{k}_i$ and $\mathbf{k}_f$, as illustrated in Fig. 1(a). For a nonspherical Fermi surface, the phonon wave vector is in general not normal to the electronic wave vectors, as shown in Fig. 1(b).

For the case of an anisotropic Fermi surface, the probability that a phonon with wave vector **q** will be absorbed by an electron depends on both the direction and magnitude of **q**. A phonon propagates through a crystal with a scattering prob-

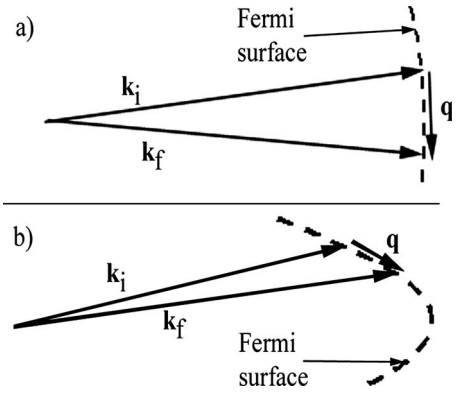

FIG. 1. Phonon absorption by scattering an electron on (a) a spherical Fermi surface and (b) a nonspherical Fermi surface.

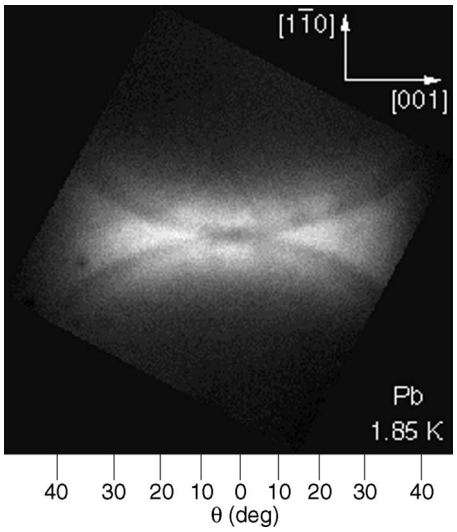

FIG. 2. Phonon image in a 1.0-mm-thick Pb crystal at 1.85 K. The center spot represents the [110] direction and the brightness indicates greater phonon flux. Angle markings indicate the angle between a phonon's group velocity and the [110] direction. The experimental raster scan has been rotated to match the crystallographic axes as in Fig. 4 and similar images.

ability that is proportional to the number of ways that its wave vector **q** connects two points on the Fermi surface. Thus, the transmission pattern of phonons emitted from a "point source" will depend on the shape of the Fermi surface.

Propagation of nonequilibrium phonons and quasiparticles across millimeter-sized Pb crystals was first observed by Narayanamurti *et al.*[2] who presented an extensive theoretical and experimental treatment of this interesting system. Using the method of phonon imaging,[3] Hauser *et al.*[4] were able to observe ballistic phonon propagation in superconducting Nb. Applying this technique to high-purity Pb single crystals cooled to about 2 K (well below the superconducting transition temperature T_c=7.2 K), Short and Wolfe[5] measured the transmission of acoustic phonons as a function of propagation direction. One of their principal results is shown in Fig. 2. This phonon image displays a remarkable set of "phonon-absorption lines" (forming the dark "*X*") that correspond to highly selective absorption of longitudinal-acoustic (LA) phonons with wave vectors in {111} planes, as described in Sec. III B 2.

The absorption lines are due to phonon scattering from quasiparticles on the anisotropic Fermi surface of Pb. In this paper we report a detailed calculation of the angular distribution of phonon-quasiparticle scattering using the accepted Fermi surface of Pb. The calculation explains the strong absorption for phonons propagating in the {111} planes, as observed in the phonon-imaging experiments.

The phonon-quasiparticle scattering rate should have a temperature dependence proportional to the quasiparticle density. BCS theory predicts that the number of quasiparticles in thermal equilibrium at temperature $T \ll T_c$ increases exponentially according to $\exp[-\Delta_o/k_BT]$,[6] where the superconducting gap parameter Δ_o acts as an activation energy for quasiparticles. The strength of the phonon-absorption lines, however, displayed a much weaker dependence[5] on lattice temperature than that predicted using the accepted gap parameter, Δ_o=1.35 meV,[7,8] for Pb. The weak temperature dependence of absorption lines seemed to be consistent with some previous measurements of ultrasound attenuation and electronic specific heat. (See Sec. IV for a discussion of these papers).

To explain an anomalous temperature dependence in Keesom and van der Hoeven's measurements[9,10] of specific heat, Overhauser and Daemen[11,12] proposed that Pb has a highly anisotropic energy gap due to a spin-density-wave (SDW) ground state. Their SDW theory predicts deep depressions (or "valleys") in the energy gap, resulting in a significant density of quasiparticles at low temperatures due to a lower activation energy for creation of quasiparticles in the valleys.

In the initial report based on a 1-mm-thick crystal,[5] Short and Wolfe suggested that the phonon-absorption lines of Fig. 2 are caused by quasiparticle scattering *within* SDW valleys (an "in-valley" process). In the present work, we have conducted experiments with crystals of 1.0 mm and 2.5 mm thicknesses, and found that the extracted absorption coefficients depend on path length, which is *not* consistent with our previous hypothesis.

In refining our understanding of phonon scattering in the presence of potential valleys in the energy gap, we have calculated the rate of phonon scattering from isotopes in Pb and determined the frequency-dependent phonon transmission probability for these two samples. We predict that if isotopes are the limiting mass defects, then a significant fraction of these ballistic phonons have energies that are capable of ejecting quasiparticles from deep valleys in the gap. Indeed, this "exit-valley" process should far outweigh "in-valley" scattering for our experimental conditions (see Fig. 17).

We define Δ_c as the threshold phonon energy required to eject a quasiparticle from a valley. Due to phonon scattering from Pb isotopes, an increasing crystal thickness implies a diminishing fraction of transmitted phonons with energy greater than Δ_c. By incorporating a quantitative model for isotope scattering, we can account for the increase in absorption coefficient with path length but the temperature dependences for the 1 and 2 mm crystals are still not in good agreement. To further test the "exit-valley" idea, we have fabricated a phonon interference filter that is designed to block the transmission of higher frequency phonons, as described in Sec. VII. Contrary to the prediction of the exit-valley model, the filter does not reduce the strength of the phonon-absorption lines, leaving little evidence for deep valleys in the superconducting gap of Pb. An explanation of the weak temperature dependences of phonon-absorption lines is left to the following paper.

In order to bring together the diverse properties of Pb that relate to the phonon-absorption lines shown in Fig. 2, this paper is divided into several sections. In the next section, we describe the experimental setup and parameters of phonon-imaging. In Sec. III A we explore the impact of isotope scattering on the frequency distribution of ballistic phonons. The momentum and energy relationships of phonon-quasiparticle scattering alluded to at the very beginning of this paper will be developed in more detail in Sec. III B. In Sec. IV, we report measurements of the strength of the absorption lines

as a function of temperature and sample thickness. Section V explores the effects of Fermi-surface anisotropy on possible SDWs in Pb. In Sec. VI we consider the frequency dependence of phonon scattering from quasiparticles in reduced-gap locations and test an interpretation of our data in terms of exit-valley scattering. Experiments with a low-pass phonon filter are described in Sec. VII.

II. PHONON IMAGING OF Pb

A. Basic techniques

The basic configuration of our phonon-imaging experiments is illustrated in Fig. 3(a). Opposite sides of the single-crystal Pb samples[13] are coated with 1000 Å films of SiO. A 2500 Å Cu film is then evaporated on the excitation side. At the center of the opposite face, we deposit an 800 Å layer of granular Al, patterned as shown in the inset of Fig. 3(b). When the sample is immersed in a bath of superfluid helium at about 2 K, the Al film acts as a superconducting bolometer. Focusing a pulsed laser beam onto the Cu film briefly heats the film, which emits phonons into the bulk of the sample. A cavity-dumped Ar^+ laser produces 10 ns pulses with energies ranging from 1 to 25 nJ that produce peak temperatures in the metal film ranging from 30 to 70 K when the laser is focused to a full width at half maximum (FWHM) of 15 μm (see analysis below).

The nonequilibrium phonons emitted from this point source are detected as a resistance change in the current-biased Al bolometer. The superconducting transition of our granular aluminum bolometers are at $T_c \approx 2.1$ K yet we can use these detectors for bath temperatures down to the lowest temperature of our cryostat—about 1.45 K. To operate at $T < T_c$, we keep the bolometer near its transition temperature by applying the appropriate bias current. Except in a small region near the bolometer, the crystal (immersed in the He bath) remains at the bath temperature. Once a desired bath temperature is reached by pumping on the liquid He, the current bias is applied to bring the central (high current-density) region of the Al film into its normal state. The bias is then carefully reduced to minimize the spatial size of the transition region. Too little bias means too little signal. Too much bias means reduced angular resolution and unnecessary generation of nonequilibrium quasiparticles in the crystal.

When the bolometer is properly biased, the phonon signal is proportional to phonon flux, which is recorded as a function of time [producing a time scan as in Fig. 3(b)] or as a function of laser position (producing a phonon image as in Fig. 2). The repetition rate of the laser pulses is typically 20 kHz. A boxcar integrator measures the average bolometer signal during some time interval (Δt) that starts at a selected gate time t_g following the laser pulse.

Due to the acoustic anisotropy of Pb, an *isotropic* distribution of k vectors emitted from a thermal source produces an *anisotropic* distribution of group velocities, an effect known as phonon focusing.[3] Calculations of the ballistic phonon-focusing pattern for longitudinal-acoustic (LA) and transverse-acoustic (TA) phonons in Pb are shown in Figs. 4(a)–4(c). In Fig. 4(d) we show an experimental phonon image taken with a broad time gate in order to show portions of the arrival of each mode. In this paper, we shall deal almost exclusively with the LA phonons, corresponding to the calculated phonon-focusing pattern shown in Fig. 4(a).

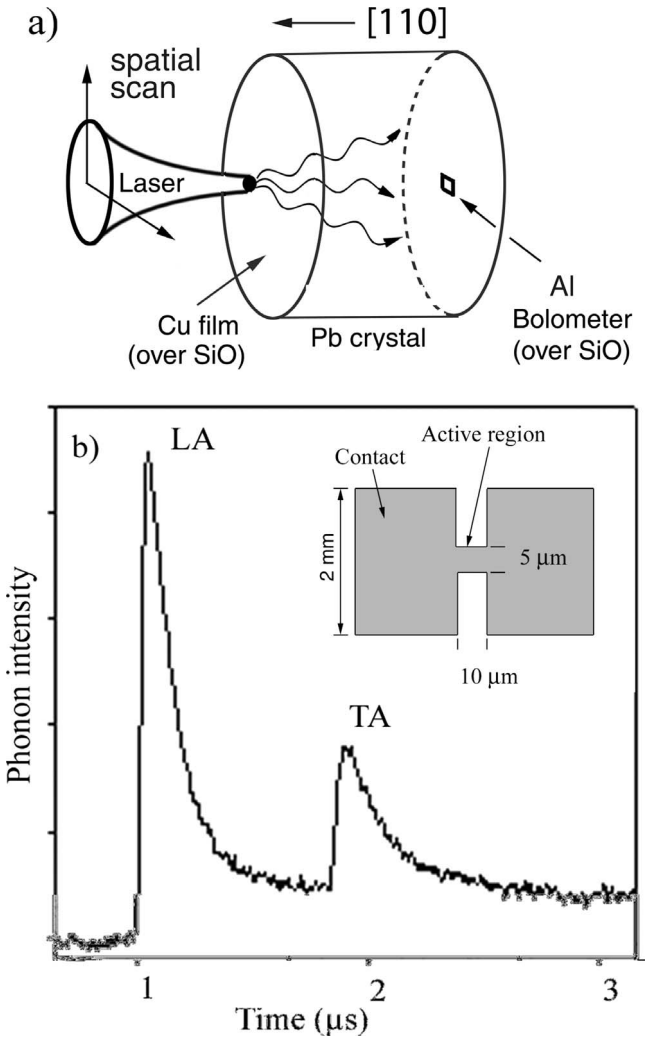

FIG. 3. (a) Illustration of phonon-imaging. The Cu film is locally heated with a focused laser pulse. On the opposite side of the crystal, a granular-Al bolometer detects the phonons traversing the sample. Scanning the laser beam in two dimensions produces a phonon image as in Fig. 2. Scanning the beam along a line produces a typical "line scan" as in Figs. 10–12. (b) A "time scan" for phonon propagation along [110] (center of the image) in a 2.5-mm-thick sample. The LA and (degenerate) TA modes arrive at times given by their group velocities. The laser has been defocused to a FWHM of 125 μm for this time scan. Inset: geometry of the bolometer with an effective dimension of 5×10 μm^2.

B. Estimating phonon frequencies

The Al bolometer is a broadband detector so we have no direct experimental measurement of the phonon frequencies present in the observed heat pulses. Nevertheless, the frequency distribution can be estimated from the input optical power density, and the acoustic emissivity of Cu into helium

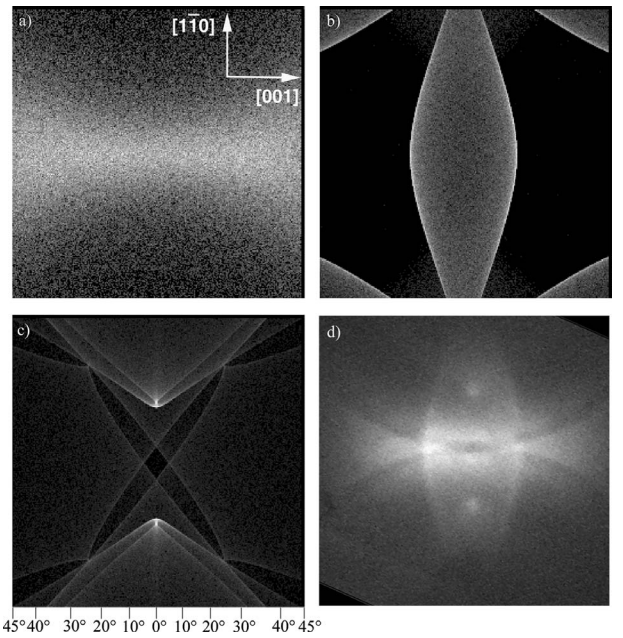

FIG. 4. Monte Carlo simulations of phonon flux through a 1.0-mm-thick, [110] oriented Pb sample for the (a) LA, (b) fast TA, and (c) slow TA modes. Scale on bottom edge of (c) gives the scale for all figures. At the center of the images (i.e., [110] propagation direction), the two transverse modes have orthogonal polarizations directed along (001) and (1$\bar{1}$0) directions. (d) Experimental phonon image of all modes in 2.5 mm of [110] Pb. The experimental image in (d) has been rotated to match the simulation orientation. Low frequency phonon focusing depends only on propagation angle, not sample thickness. For parts (a)-(c) and later computations, we use the low-temperature elastic constants of Pb: $C_{11}=5.554\times10^{11}$, $C_{12}=4.542\times10^{11}$, and $C_{14}=1.942\times10^{11}$ dyne/cm^2 (Ref. 14). The pattern of phonon caustics is well described by the (nondispersive) continuum model.

and Pb. This standard calculation, as applied to our case, is briefly described below.

Power transmission into the Pb crystal occurs at a rate given by the Stefan-Boltzman Law for phonons,[15]

$$\frac{P}{A}=\sigma(T_r^4-T_s^4)=\frac{\pi^5k_B^4}{15\hbar^3}\left(\frac{\epsilon_L}{v_L^2}+\frac{\epsilon_{FT}}{v_{FT}^2}+\frac{\epsilon_{ST}}{v_{ST}^2}\right)(T_r^4-T_s^4), \quad (1)$$

where P/A is the absorbed "power density" and σ is the Stefan-Boltzman constant for phonons. The v's are phonon velocities and ϵ's are spectral emissivities between radiator, r, and substrate, s. Accounting also for losses into both the helium bath and Pb sample, and assuming the sample and helium bath are at the same temperature, T_s, we find the steady-state temperature in the Cu film to be[16]

$$T_r=\left[\frac{P_{\text{laser}}}{A(\sigma_{\text{Cu/He}}+\sigma_{\text{Cu/Pb}})}+T_s^4\right]^{1/4}. \quad (2)$$

Emissivities between two solids, or between a solid and liquid helium, are generally equal to about 50% due to diffuse scattering at an interface. Therefore, we assume $\epsilon=0.5$ for all the emissivities in this rough estimate.[17]

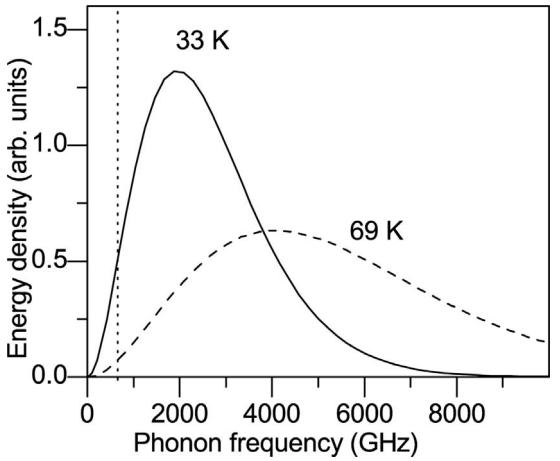

FIG. 5. Planckian energy distribution for 33 and 69 K source temperatures. The curves have been normalized to have the same total energy, representing the change in distribution for a 50 nJ pulse of energy deposited with differing focus conditions. The vertical dotted line is the frequency of a $2\Delta_o$ phonon.

With the average acoustic velocities for Cu, we obtain $\sigma_{\text{Cu/He}}=322$ W/m^2 K^4 and $\sigma_{\text{Cu/Pb}}=400$ W/m^2 K^4. For a laser-pulse length of 15 ns, and typical (absorbed) excitation energies of 1.5 and 24 nJ onto a spot with FWHM $=15$ μm, the calculated temperatures of the copper film are 33 and 69 K, respectively. Figure 5 shows the corresponding Planck distributions of phonon energy density versus frequency. If the copper film were instead isolated from its surroundings, it would reach a temperature about three times as high as the steady-state temperatures calculated above. More details may be found in Refs. 3 and 18.

C. Phonon source

The vertical dotted line in Fig. 5 indicates the $2\Delta_o/h$ frequency for LA phonons in Pb. Phonons with energy greater than $2\Delta_o$ rapidly break Cooper pairs and thus have a small mean-free path. This means that, for the focused laser condition considered above, a large part of the thermal energy emitted by the metal film will be absorbed by pairbreaking in superconducting Pb near the Cu-Pb interface.

The situation near the phonon source is quite complicated. Energetic quasiparticles created by high-frequency phonons lose their kinetic energy by emitting lower frequency phonons, which in turn scatter frequently, possibly producing a "hot" phonon/quasiparticle cloud near the excitation point. At sufficient laser power, the localization of electronic and vibrational energies likely produces a small region of normal metal in the superconductor. For example, 1 nJ of energy is sufficient to heat a $10\times10\times10$ μm^3 cube of Pb from 2 K to its critical temperature of 7.2 K.[18] At our highest energies of 24 nJ and a 10 μm focused laser spot, a localized hot spot exhibits a lifetime of roughly 0.5 μs, as described in Ref. 18.

Narayanamurti *et al.*[2] observed ballistic and diffusive propagations of thermal energy in pure Pb crystals but the effect was observed at lower power densities and higher crystal temperatures than reported here. At temperatures

greater than 3 K, for example, the *ambient* phonon population provides a highly diffusive medium for the nonequilibrium quasiparticles, resulting in a diffusive quasiparticle/phonon cloud. It is possible that such an effect could be happening near our phonon source where the nonequilibrium quasiparticle density is high.[18] At our highest excitation energies (24 nJ), a small signal starting before the ballistic phonon onset is observed. This supersonic signal will be analyzed in Sec. V of the following paper.

In the rest of this paper we confine ourselves to sampling times, $t_b < t < 1.5t_b$, where the phonon source is quite localized, and t_b is the ballistic arrival time of LA phonons along {110}. Next we consider the propagation of phonons through the bulk of a cold Pb crystal.

III. PHONON SCATTERING PROCESSES

A. Mass defect scattering

Phonons scatter from defects in the periodic crystal lattice. The most common form of defect is the random occurrence of atomic isotopes. The phonon-scattering rate from isotopes—i.e., Rayleigh scattering—increases with the fourth power of the phonon frequency:[3]

$$\tau_{\rm iso}^{-1} = A_I \nu^4, \tag{3}$$

where $A_I = 4\pi^3 V_o g / v^3$ depends on the cell volume per atom V_o, the average phonon velocity v, and the mass-disorder factor g. Following the calculations of Tamura[19] and using the appropriate isotope values for Pb,[20] we find that $A_I = 5.052 \times 10^{-41}$ s^3. The corresponding isotopic scattering times and mean-free-path for LA phonons are plotted in Fig. 6(a).

The transmission function against isotope scattering for LA phonons is given by $T(\nu) = \exp\{-L/[v_L \tau_{\rm iso}(\nu)]\}$. In Fig. 6(b) we show that only a small fraction of phonons originating from a 69 K Planck distribution are able to travel ballistically (without scattering from isotopes) across a 2.5 mm crystal of Pb. Indeed, the frequency distribution of the ballistically transmitted phonons hardly depends on the source temperature, provided that $k_B T_{\rm source}/h$ is much higher than the "cut-off" frequency due to isotope scattering, about 400 GHz from Fig. 6(b). This effect is shown clearly in Fig. 7, which also shows that the frequency distribution of phonons reaching the detector ballistically depends significantly on the crystal thickness.

Is the scattering from mass defects in the crystal really limited by isotopic randomness? What about impurities? The crystal has a nominal atomic purity of 99.9999%.[13] Assuming the greatest possible mass defect for each impurity site, we find a mass-defect factor g that is 20 times less than that for naturally occurring isotopes. However, structural defects such as vacancies, interstitial atoms, and dislocation lines could conceivably dominate isotopic scattering of phonons in Pb. We now turn to the principal topic of our study.

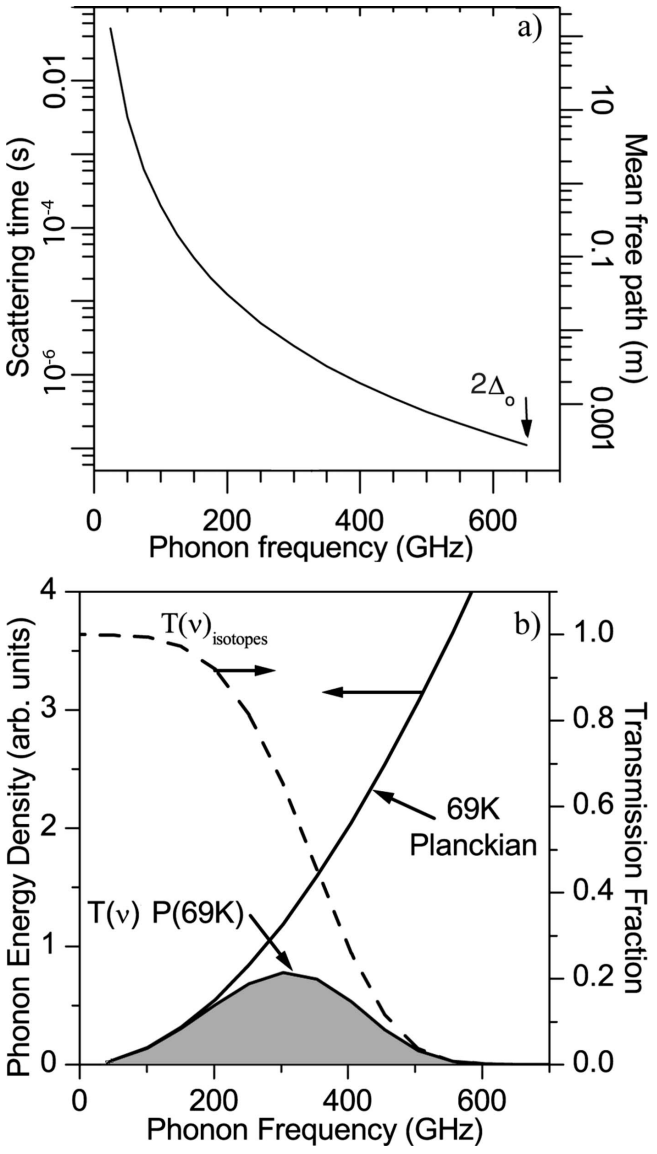

FIG. 6. (a) Phonon scattering time versus frequency due to isotope variations in Pb. Right axis gives the mean-free path of a [110] LA phonon with $v = 2.5$ mm/μs. (b) The solid line gives the Planckian distribution of phonons for a 69 K source. The transmission function for isotope scattering in a 2.5 mm sample is the dashed line. The shaded area is the expected LA phonon distribution at a detector 2.5 mm from the source. Notice that the distribution of LA phonons arriving at the detector is less than 650 GHz, which is the $2\Delta_o/h$ frequency in Pb, neglecting absorption by quasiparticles.

B. Scattering from quasiparticles

1. Spatially averaged rate

Although subgap phonons (those with energy less than $2\Delta_o$) are unable to break Cooper pairs, they are quite capable of scattering from thermally excited quasiparticles. The equilibrium density of quasiparticles has a temperature dependence given by the Fermi-Dirac distribution function, $f(\omega)$, where $\omega = E_{qp}/\hbar$ with E_{qp} as the kinetic energy of a quasiparticle. Kaplan *et al.*[21] derived the following formula for the scattering rate of a phonon with angular frequency Ω from equilibrium quasiparticles:

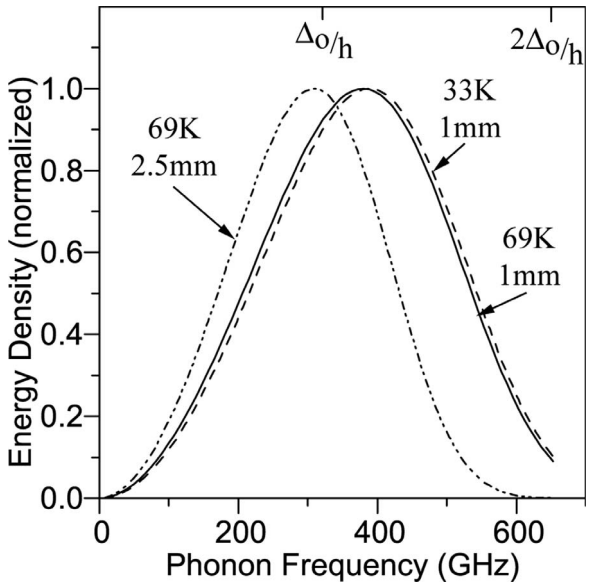

FIG. 7. Normalized phonon distributions arriving at the detector for three combinations of source temperature and sample thickness. Notice that the sample thickness is more important to the distribution arriving at the detector than the source temperature. This calculation neglects absorption by quasiparticles.

$$\tau_{ph-qp}^{-1}(\Omega) = \frac{8\pi N(0)\alpha^2(\Omega)}{\hbar N} \times \int_{\Delta}^{\infty} \frac{d\omega}{(\omega^2-\Delta^2)^{1/2}} \frac{\omega(\Omega+\omega)+\Delta^2}{[(\Omega+\omega)^2-\Delta^2]^{1/2}} \times [f(\omega)-f(\Omega+\omega)], \quad (4)$$

where $N(0)$ is the normal-metal density of states at the Fermi surface, N is the spatial density of conduction electrons, $\alpha^2(\Omega)$ is a measure of electron-phonon coupling, and Δ is the *temperature-dependent* superconducting gap parameter. Kaplan *et al.* computed a characteristic phonon-scattering time τ_o^{ph} using the average coupling strength and other parameters for Pb,

$$\tau_o^{ph} \equiv \hbar N/4\pi^2 N(0)\langle\alpha^2\rangle_{av}\Delta(0) = 0.340 \times 10^{-10}\ \text{s}. \quad (5)$$

Using this value, we plot the temperature dependence of τ_{ph-qp} in Fig. 8(a).

The vertical lines in Fig. 8(a) indicate the range of temperatures relevant to our present experiments. Between 1.4 and 2.1 K, the predicted phonon-scattering time, τ_{ph-qp}, ranges from about 15 μs down to 0.3 μs. At 2.1 K, τ_{ph-qp} is comparable to the 0.4 μs ballistic time of flight for LA phonons crossing the 1 mm crystal. Notice in Fig. 8(b) that, according to this model, phonons with energies between $0.2\Delta_o$ and $2\Delta_o$ have scattering times that are only weakly dependent on the phonon energy.

2. Anisotropy in phonon absorption

As discussed in Sec. I, the angular distribution of phonon absorption depends on the particular shape of the Fermi surface for a material. An acoustic phonon is absorbed by scattering a quasiparticle from one point on this surface to another so we must examine the shape of the Fermi surface of Pb in detail.

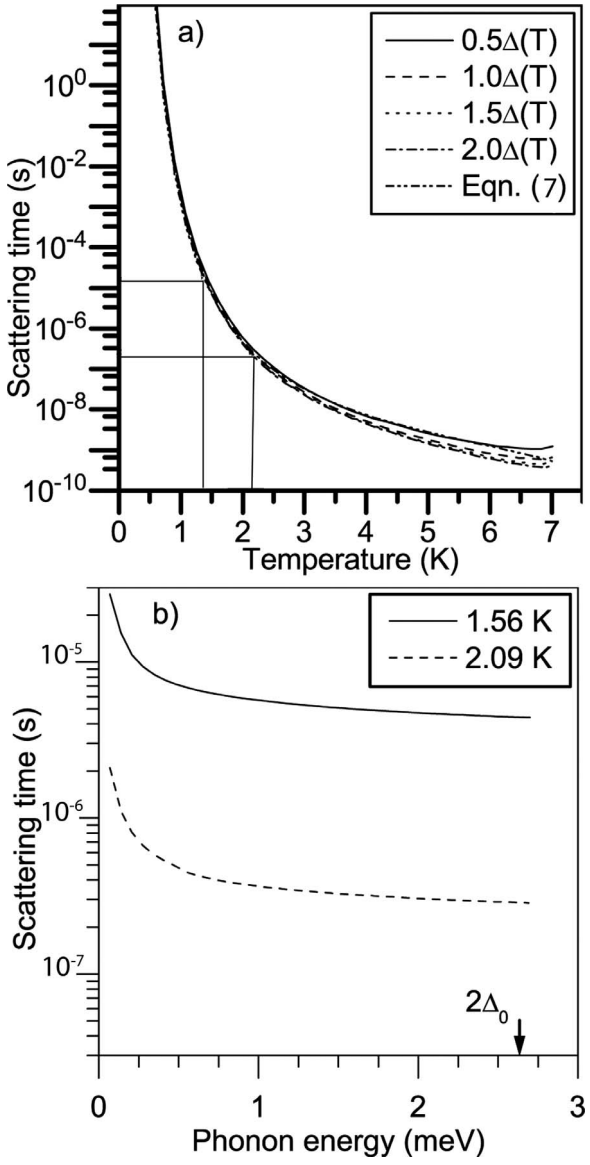

FIG. 8. (a) Phonon-quasiparticle scattering time versus temperature for four subgap LA phonon energies calculated using Eq. (4). Also plotted is the scattering time calculated using Eq. (7). Vertical lines bound the temperature range studied in our experiments. (b) Scattering time versus LA phonon energy at 1.56 and 2.09 K sample temperatures.

The Fermi surface is best illustrated by considering separately the portions in the second and third zones. The hole-like portion in the second zone forms a rounded octahedral shape when plotted in the reduced-zone scheme shown in Fig. 9(a). The third-zone portion of the Fermi surface forms a network of tubes and is shown in Fig. 9(b).

The tight-binding calculations of the Fermi surface from Ref. 22 shown in Figs. 9(a) and 9(b) are based solely on tight-binding theory, and were not adjusted to fit experimental data. Although we find these images very useful for visualization, in our work we model the Fermi surface after the

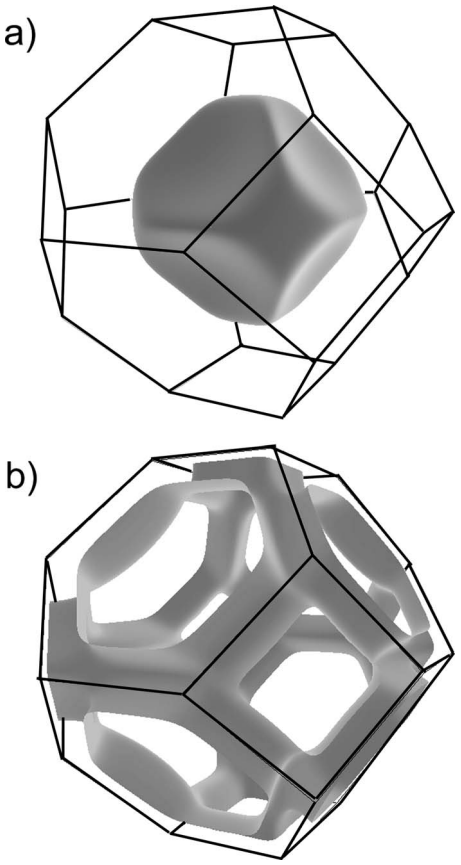

FIG. 9. The (a) second-zone and (b) third-zone portions of the Fermi surface of Pb calculated using a tight-binding calculation, and plotted in a reduced-zone scheme by Choy *et al.* (Ref. 22).

classic study of Anderson and Gold.[1] They fit de Haas-van Alphen data to a pseudopotential model with four orthogonal plane waves including spin-orbit coupling. In the calculations that follow, we use their equations and fitting parameters to calculate the magnitude of electronic wave vectors $\mathbf{k}(\theta,\phi)$ that define the Fermi surface of Pb.

Using a Monte Carlo technique, we examine the scattering of the subgap phonons with quasiparticles or unpaired electrons. This scattering depends sensitively on the phonon propagation direction. A spatial pattern of absorbed phonons is accomplished by first generating a random angular distribution of electronic wave vectors. If the momentum difference, $\mathbf{q}=\mathbf{k}_f-\mathbf{k}_i$, between a pair of states on the Fermi surface corresponds to the momentum of a phonon with energy $h\nu$ less than $2\Delta_o=2.7$ meV, then we compute the group velocity of this phonon and mark with a black dot where it would have arrived in the absence of quasiparticle scattering. In fact, this dot represents a phonon that is *absorbed* by a quasiparticle so the pattern of dots generated by many such random events corresponds to an absorption pattern for the phonons.

LA phonons with $h\nu<2\Delta_o$ have wave vectors less than one tenth the radius of the Fermi sphere, corresponding to an angle of 6° between $\mathbf{k}_i$ and $\mathbf{k}_f$. Thus, we find that absorption patterns are relatively insensitive to phonon frequency.

Figure 10(a) shows the calculated absorption pattern for phonons with ($h\nu<2\Delta_o$) that were absorbed by quasiparticles on the second zone of the Fermi surface. Figure 10(b) is a high-resolution phonon image of the 2.5 mm Pb crystal showing excellent agreement between the absorption lines and the theory of part (a).

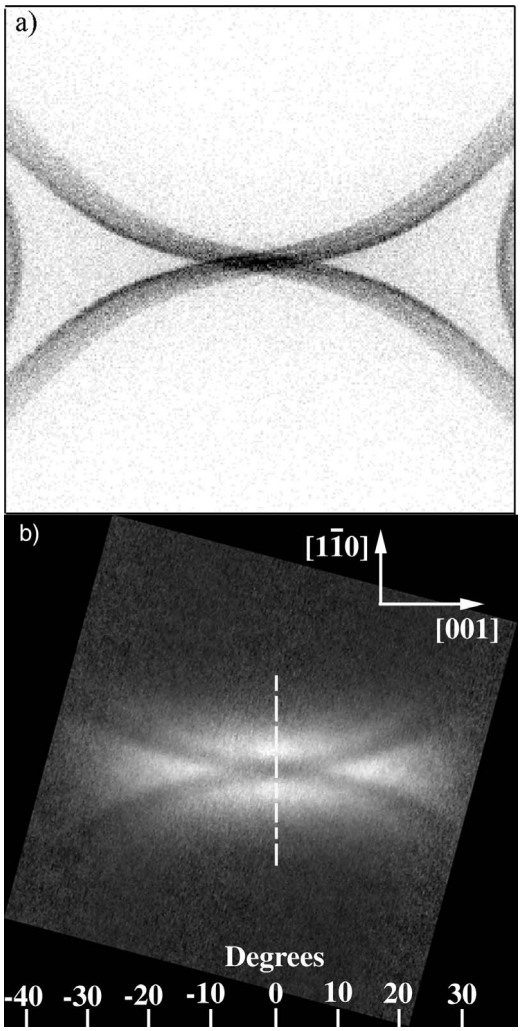

FIG. 10. (a) Predicted absorption patterns of LA phonons with $h\nu<2\Delta_o$ caused by electrons on the second zone of the Pb Fermi surface. The dark bands represent a reduction in ballistic phonon flux and correspond closely to phonons with wave vectors in {111} planes. The lines are curved due to phonon focusing, whereby wave vector and group velocities are not collinear. (b) LA phonon image in the 2.5 mm sample at 2.09 K. A time gate of 0.5 μs centered at $t=1.25$ μs was used for this image. Angles on the lower axis indicate the angle between phonon group velocity and [110]. The dashed line shows the path of our standard line scan, corresponding to Figs. 11 and later.

The absorption pattern in Fig. 10(a) can be understood by considering the shape of the second-zone surface, as shown in Fig. 9(a). This octahedral-like surface has large, relatively flat regions that are nearly {111} planes. Consequently, the wave vectors of the absorbed phonons, which are tangent to this surface, lie roughly in the {111} planes, corresponding to the experimental absorption lines.

Phonons scattered from quasiparticles in the third zone add little to the overall absorption pattern.[18] Consider the tubular structure shown in Fig. 9(b). Phonons connecting $\mathbf{k}_i$

and $\mathbf{k}_f$ on the same tube lead to a small concentration of scattered wave vectors nearly along [110]. Phonons connecting $\mathbf{k}_i$ and $\mathbf{k}_f$ on adjacent tubes lead to a very diffuse pattern of scattered wave vectors.

Finally, the second-zone and third-zone surfaces are separated by a minimum distance in k space of 2.2×10^7 cm^{-1}, which is greater than the maximum wave vector of a subgap LA phonon. Hence the absorption of a subgap LA phonon cannot involve the transition of an electron from one zone to the other.

From this analysis of phonon-scattering mechanisms in Pb, there is little doubt that the absorption lines observed in the experimental phonon images are caused by scattering from quasiparticles on the Fermi surface. In Ref. 18, Short showed that the predicted SDW valleys would most likely lie in the {111} "flats" of the second zone of the Fermi surface; therefore, only phonons propagating nearly along {111} planes would be absorbed by quasiparticles in the valleys (see also Fig. 15). Consequently, the observed *anisotropy* of phonon absorption is not evidence for the existence of SDWs. Instead, it is our preliminary temperature dependences of the absorption coefficient, based on the assumption of quasiparticles in thermal equilibrium with the lattice, which suggest the possibility of deep valleys in the superconducting gap, as shown below.

IV. ANOMALOUS TEMPERATURE DEPENDENCE OF QUASIPARTICLE DENSITY

The commonly accepted method for determining the superconducting gap is electronic tunneling between a metal film and the superconductor through an insulating layer.[7] Tunneling studies in Pb have revealed a multiple-gap structure[23,24] associated with the two sheets of the Fermi surface and theoretical calculations[25–28] are in reasonable agreement with these measurements. In these studies, the gap parameter exhibits an anisotropy of at most 10%. Overhauser and Daemen[29] have pointed out that standard tunneling experiments are not well suited for observing sharp dips in the gap structure, and they analyzed the possibility of SDW effects in quench-condensed films.[30,31]

According to BCS theory, at temperatures well below the superconducting transition temperature $T_c=7.2$ K, the electronic specific heat has the form

$$C_{es} = a\gamma T_c \exp(-bT_c/T), \tag{6}$$

where a and b are material-dependent parameters. BCS theory also gives the relation between T_c and Δ_o so the temperature dependence of C_{es} provides a measure of the superconducting gap. To extract the specific heat associated with thermally excited quasiparticles (C_{es}), it is necessary to account for the normal-state specific heat (C_n) that is measured at $T\ll T_c$ by applying a magnetic field that destroys the superconductivity.

Van der Hoeven and Keesom[9,10] reported a low-temperature electronic specific heat far above the BCS prediction for high-purity superconducting Pb—an effect that was not present for crystals doped with a few percent indium. However in a discussion of Ref. 32, Keesom[33] pointed out that it was an anomalous normal-state specific heat in their original experiment that changed with indium doping, not the superconducting-state specific heat. In contrast, the low-temperature study by Phillips *et al.*[32] shows no anomalous behavior in either the normal or superconducting specific heat of pure Pb.

A third experimental technique that is sensitive to the superconducting gap is ultrasonic attenuation. According to standard BCS theory, the ratio of the acoustic attenuation coefficient for the superconducting state to that of the normal state is given by[6]

$$\frac{\alpha_s}{\alpha_n} = 2f(\Delta/kT) = \frac{2}{\exp(\Delta/kT)+1}, \tag{7}$$

where $f(\Delta/kT)$ is the Fermi-Dirac distribution function. For $k_BT\ll\Delta$, the attenuation increases exponentially with temperature due to the rise in the number of thermally excited quasiparticles.[34]

In a conventional ultrasound experiment, the attenuation of an acoustic wave is determined from the diminishing amplitude of multiple reflected pulses, assuming that the reflection coefficient is known. Conveniently, ultrasound is easily transmitted through both superconducting and normal materials, allowing one to obtain the ratio α_s/α_n of attenuation coefficients and test the predictions of Eq. (7). Unfortunately, coherent ultrasound suffers from a sensitivity to dislocations that is particularly acute for an easily deformable Pb crystal.[35]

Using ultrasonic attenuation, Fate *et al.*[36,37] observed significant deviations from the expected strong-coupling BCS behavior at low temperatures in Pb, possibly indicating an unusual gap anisotropy. On the other hand, Tittmann *et al.*[38] did find agreement with the normally accepted BCS gap behavior for Pb. As explained in Ref. 35, the high amplitudes of coherent sound waves lead to an amplitude-dependent ultrasound absorption due to dissipative dislocation motion. Plastic deformation of a crystal reduces this amplitude-dependent effect[36,37] by restricting dislocation motion but leaving a residual attenuation at low amplitudes. Instead of deforming a high-purity crystal, Tittmann *et al.*[38] introduced 0.1% tin impurities to pin the dislocations. Under these conditions, they observed a superconducting gap consistent with BCS.

In phonon-imaging experiments, one must determine the fraction of absorbed phonons from a single transit across the crystal. Furthermore, due to strong electron-phonon scattering in the normal state, ballistic transit is only possible when the crystal is in the superconducting state. The advantage of phonon-imaging, however, is that the strength of the absorption lines is directly related to the number of quasiparticles along the phonon path.

A measure of the phonon absorption along the [110] direction is obtained by recording a "line scan" across the center of the phonon pattern, as indicated by the dashed line in Fig. 10(b). Such line scans at 1.6, 1.8, and 2.0 K are plotted in Fig. 11. These data clearly show that the fraction of absorbed phonons (the depth of the dip) is increasing with temperature; however, there is only a factor of about two change in the absorbed fraction, much less than that predicted by Eq.

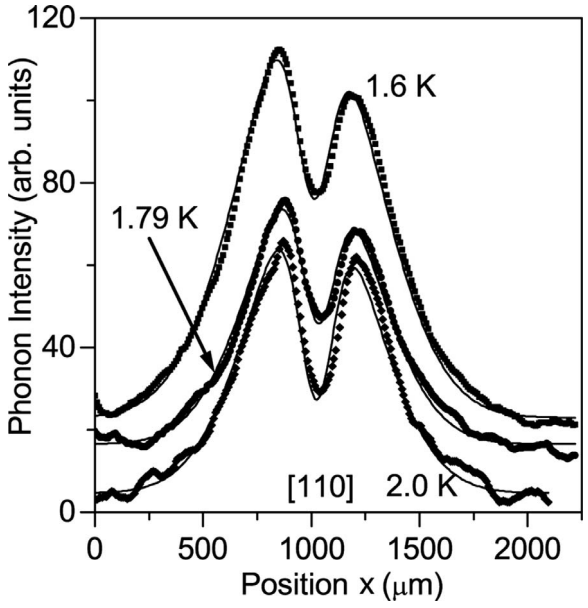

FIG. 11. Line scans through the center of the phonon pattern, as indicated by the dashed line in Fig. 10(b) at 1.6, 1.79, and 2.0 K. Notice the increasing depth of the depression around [110] as the sample temperature increases.

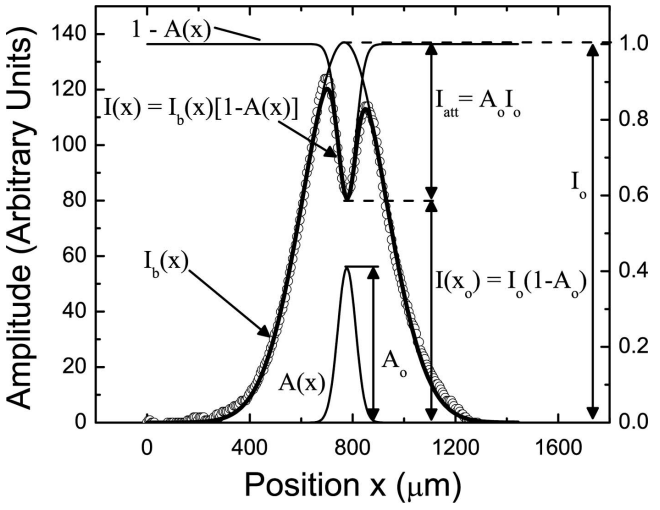

FIG. 12. Line scan through [110] and fit to Eq. (11) (solid line through the data points) at 1.85 K in a 1 mm sample. The Gaussian $I_b(x)$ with amplitude I_o represents the expected ballistic phonon signal in the absence of the absorption process. The function $A(x)$ (dotted line with amplitude given on the right vertical axis) is the fraction of phonons absorbed as a function of direction. Multiplying the transmission function $[1-A(x)]$ and the expected signal $I_b(x)$ together results in the function $I(x)$ used to fit the data.

(7). With the generally accepted gap $\Delta_o=1.35$ meV for Pb,[7,8] this equation predicts a factor of ten increase in absorption as the temperature is raised between 1.5 and 2.0 K, which is roughly our experimental temperature range. This puzzle will occupy our attention for most of the rest of this paper.

Throughout our analysis, we will concentrate on the fraction of phonon flux that is absorbed along the [110] propagation direction, i.e., reduction in intensity at the center of the X in Fig. 10(b). A vertical line scan through the center of the pattern [i.e., in a (100) plane] produces a spatial profile like the one shown in Fig. 12. This line scan is composed of two basic distributions: (a) the profile $I_b(x)$ associated with the focusing of ballistic LA phonons in the (100) plane and (b) the profile $A(x)$ characterizing the absorbed fraction of phonons in this plane. Figure 12 shows that the two functions are empirically well described by the Gaussian functions

$$I_b(x) = I_o \exp[-(x-x_o)^2/2\sigma_o^2], \tag{8}$$

and

$$A(x) = A_o \exp[-(x-x_o)^2/2\sigma_a^2], \tag{9}$$

The transmission function for phonons with wave vectors in this plane is given by $[1-A(x)]$; therefore, the net phonon flux is

$$I(x) = I_b(x)[1-A(x)], \tag{10}$$

which, along the [110] direction ($x=x_o$), becomes

$$I(x_o) = I_o(1-A_o). \tag{11}$$

In the following paper we show that the near-Gaussian form of the ballistic transmission profile $I_b(x)$ results from the phonon-focusing profile convolved with time-of-flight selection by a boxcar gate. The experimental line scan, shown as the circles in Fig. 12, fit very well to Eq. (10) with adjustable parameters I_o, A_o, σ_o, and σ_a.

According to the calculation of Kaplan *et al.*[21] (see Fig. 8), the rate of phonon scattering from quasiparticles on the Fermi surface of Pb is only weakly dependent on phonon frequency. Using this result, we define a single absorption coefficient α in the usual way,

$$I(x_o) = I_o \exp(-\alpha L), \tag{12}$$

where the thickness of the crystal is L, which equals the path length along [110]. In writing this equation, we have also assumed that the scattering occurs homogeneously in the bulk of the sample, an assumption that we will reconsider later. Rearranging this equation, we solve for the absorption coefficient

$$\alpha = (-1/L)\ln[I(x_o)/I_o] = (-1/L)\ln(1-A_o) \tag{13}$$

in terms of the absorbed fraction A_o.

Solid curves in Fig. 11 are fits to Eq. (10) for data from the 2.5 mm crystal. From similar line scans in the entire data set, we obtain the temperature dependence of the absorption coefficient $\alpha(T)$ shown in Fig. 13 for the two crystal thicknesses. As in the case of ultrasonic attenuation, the absorption coefficient should be related to the effective energy gap, Δ_{fit}, by the formula,

$$\alpha(T) = a \exp(-\Delta_{\text{fit}}/k_B T), \tag{14}$$

representing the thermal creation of quasiparticles across the gap. Over the temperature range of 1.5–2.1 K, the absorption coefficient for the 2.5 mm sample is described by an energy gap $\Delta_{\text{fit}}=\Delta_o/3.6$.[39] This result is suggestive of quasiparticle

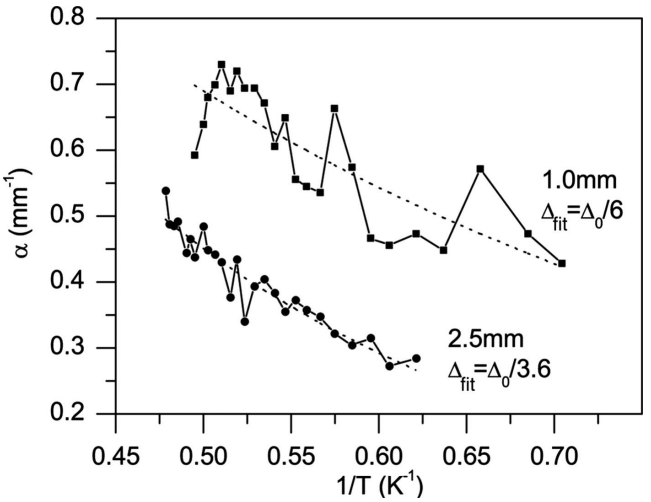

FIG. 13. Absorption coefficient $\alpha(T)$ plotted versus $1/T$ for 1 and 2.5 mm samples. The dashed lines are fits of each data set to Eq. (14) with a and Δ_{fit} as free parameters. The value of the fitting parameter Δ_{fit}, which should correspond to the minimum superconducting gap parameter, differs by a factor of 1.6 and the overall magnitude of the absorption coefficient is significantly different for each sample.

activation across a lowered gap, possibly due to anisotropy in the gap parameter.

When the same analysis is applied to the 1 mm crystal, however, a different result is obtained. The temperature dependence of α is now somewhat slower with $\Delta_{\text{fit}}=\Delta_o/6$ but, more importantly, the magnitudes of α over this temperature range are considerably higher than those of the 2.5 mm crystal. The disparity (about a factor of two) implies that Eq. (13) is too simplistic a description of the phonon flux absorption coefficient.

The weak dependence of α on temperature suggests that the superconducting gap in Pb may have strong depressions, causing an enhanced thermal population of quasiparticles. If so, the dependence of α on crystal thickness suggests that only a subset of the ballistic phonons (possibly selected by frequency) is absorbed by quasiparticles and that the fraction of phonons in this subset changes with path length. To test these ideas, we now examine in detail the possible effect of an SDW on the Fermi surface in Pb.

V. GAP ANISOTROPY DUE TO SPIN DENSITY WAVES

A. Spin density waves for a spherical Fermi surface

In an effort to explain the anomalous acoustic attenuation and specific heat in Pb, Overhauser and Daemen[11,12] proposed that the ground state of Pb is an SDW. The key point of their hypothesis is that a SDW breaks the time-reversal symmetry of standard Cooper pairs. Instead of Cooper pairing between states $\mathbf{k}\uparrow$ and $-\mathbf{k}\downarrow$, a (spiral) SDW results in pairing of $\mathbf{k}\alpha$ with $-\mathbf{k}\beta$, where α and β are mostly spin-up and spin-down states. This mixing of spin states reduces the pairing interaction strength and causes gap reductions for specific $\mathbf{k}$. Different polarizations, linear or spiral, of the

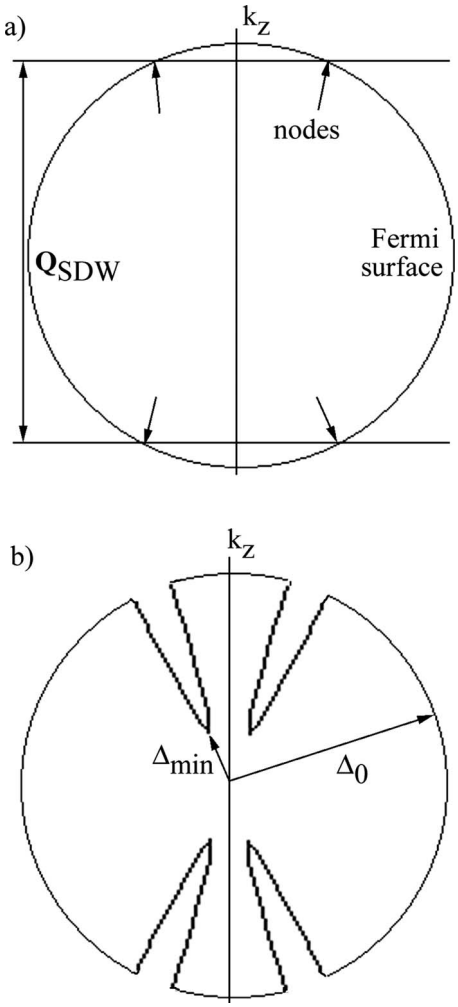

FIG. 14. (a) Short arrows indicate locations of SDW gap nodes (depressions) for a spherical Fermi surface. (b) Sketch of a polar plot of the energy-gap amplitude as a function of $\mathbf{k}$ *direction*. The angular width of the nodes has been exaggerated for clarity.

SDWs result in either nodes or small, but finite, minima in the energy gap, respectively.[39]

The basic idea of Overhauser and Daemen is illustrated in Fig. 14 for an SDW with wave vector $|\mathbf{Q}|=Q_z\approx 2|k_F|$.[40] The directions of gap minima (or valleys) correspond to electrons on the Fermi surface with $k_z=\pm Q/2$. For a spherical Fermi surface, electrons that satisfy this momentum condition lie along two rings for each SDW direction. The rings are the result of the intersection of $k_z=\pm Q/2$ planes with the spherical Fermi surface.

Because there is no evidence of SDWs in the NMR or neutron-diffraction data of Pb, Overhauser and Daemen suggested that the SDW must be commensurate with the lattice. Also, the largest effect should occur for $\mathbf{Q}\approx 2k_F$. They concluded that the SDWs in Pb are either a family of twelve [211] SDWs with magnitude $(2\pi/a)|211|\approx 0.987(2k_F)$, where $a=4.90$ Å is the lattice spacing, or possibly a family of twelve [210] SDWs with magnitude $(2\pi/a)|210|\approx 0.90(2k_F)$. The expected "node lines," or valleys, for these two cases are shown as the light rings in Fig. 15.

Depending on their depth and width, valleys of lowered gap could significantly increase the total number of ther-

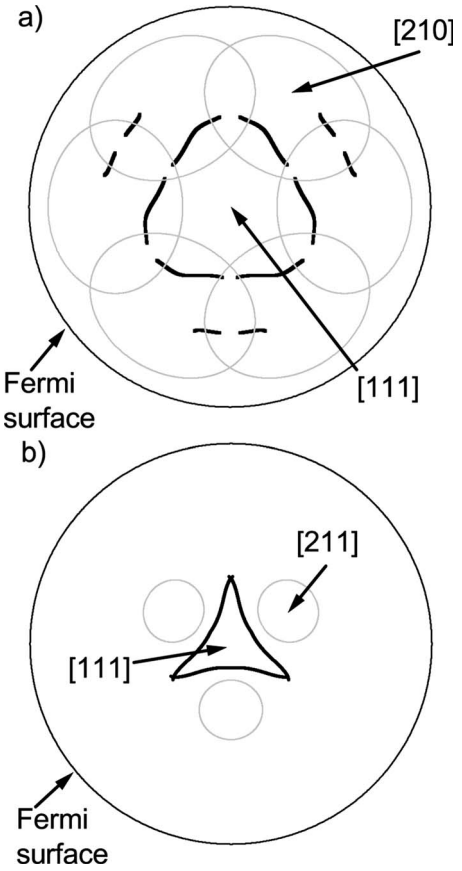

FIG. 15. Calculated directions of gap minima (valleys) due to (a) [210] and (b) [211] SDWs. Solid, thick lines are predictions based on the actual Fermi surface of Pb. Light gray lines are based on a spherical Fermi surface. We use the term "node structure" to describe these directions of lowered gap even for the case of nonzero minima.

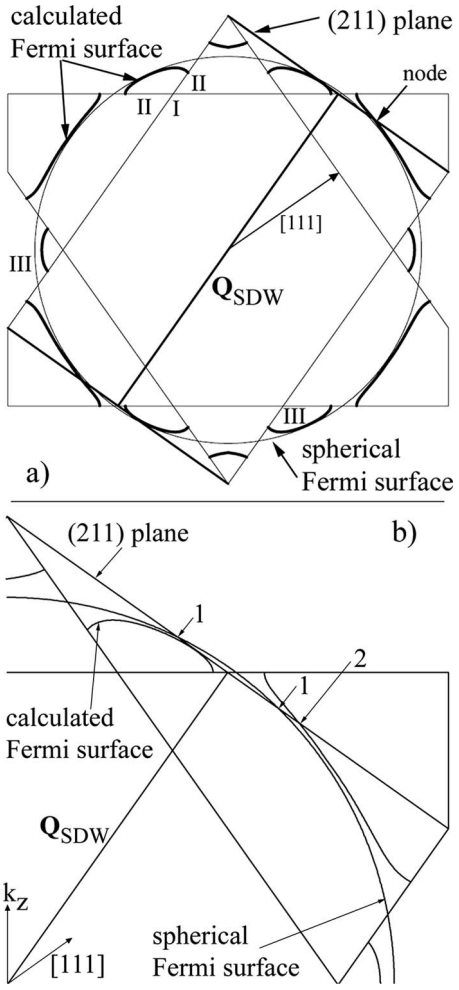

FIG. 16. (a) Cross section in the (110) plane of the Brillouin zone, spherical Fermi surface (light line), and calculated Fermi surface (dark line segments). A commensurate [211] vector is shown with two (211) planes at its end points. Intersections of these two planes and the Fermi surface are predicted locations of strong gap anisotropy due to a [211] SDW. (b) Detail of the upper right quadrant of (a) to clarify that a (211) plane crosses the spherical Fermi surface at two points, labeled 1, but only once for the calculated surface, labeled 2.

mally produced quasiparticles at low temperatures. We will consider the scattering of phonons with quasiparticles in SDW-induced valleys but first let us consider the locations of reduced gap, taking into consideration the actual Fermi surface of Pb.

B. Spin density waves for the anisotropic Fermi surface of Pb

For a linear SDW with wave vector $\mathbf{Q}$, the approximate eigenfunctions of the one-particle Hamiltonian are superpositions of plane waves with wave vectors $\mathbf{k}$ and $\mathbf{k} \pm \mathbf{Q}$. As a result, a reduced gap occurs for pairs of electronic states on the FS that are separated by momentum $\mathbf{Q}$. For a spherical Fermi surface, states with $k_z = \pm Q/2$ automatically have the required pair state at $k_z = \mp Q/2$. However, the pairing condition is not so easily met for a nonspherical surface. In this discussion we define the z axis along the SDW wave vector.

Using the numerical model of Anderson and Gold,[1] we can generate a collection of points on the anisotropic Fermi surface that coincide with $k_z = \pm Q/2$ planes. The intersections of the {210} and {211} planes with the second-zone portion of the Fermi surface are shown as the dark lines in Fig. 15, corresponding to the predicted nodes or valleys. We have projected the directions of these node lines onto a sphere that also shows the node lines for the spherical Fermi surface as light circles.[18]

Figure 16(a) is a (110) cross section of the Fermi surface and the Brillouin-zone boundaries. For reference, the thin line shows the dimension of the spherical Fermi surface of Pb. The figure shows a commensurate [211] SDW wave vector, which is bounded by two (211) planes that define $k_z = \pm Q/2$. Extending the reasoning of Overhauser and Daemen, we expect the intersection of these two planes with the Fermi surface to be close to the locations of gap depressions.

An expansion of the cross section, shown in Fig. 16(b), demonstrates that the (211) plane would intersect a spherical Fermi surface at the two points labeled "1" but it crosses the actual Fermi surface at only one point, labeled "2." This behavior is consistent with the circles in Fig. 15(b) breaking into line segments. Notice that the (211) plane is nearly tan-

gent to, but actually does not touch, one portion of the Fermi surface.

VI. PHONON ABSORPTION IN THE PRESENCE OF GAP ANISOTROPY

Let us now consider the scattering of phonons from quasiparticles thermally excited into narrow regions of reduced gap. Phonons with energies less than $\Delta_c=\Delta_o-\Delta_{\min}$ would have frequencies near 230 GHz if $\Delta_{\min}\approx\Delta_o/4$, as suggested by van der Hoeven and Keesom.[10] These phonons have momenta $\mathbf{q}=5.9\times10^6$ cm^{-1} that represents about 4% of the Fermi momenta for a quasiparticle and they make up a significant fraction of phonons crossing the sample ballistically, as can be seen in Fig. 6. Phonons with energy less than Δ_c are restricted to scattering a quasiparticle from one part of the node structure (heavy lines in Fig. 15) to a nearby portion of the node structure—a process shown in Fig. 17(a) and labeled "in-valley"—as the phonon has insufficient energy to eject the quasiparticle from the valley.

Our previous report[5] considered only these in-valley events, which include the intravalley and intervalley processes shown in Fig. 17(a). Only intervalley scattering between the intersecting segments of the triangle in Fig. 15(b) produced a broad angular range of phonon absorption in {111} planes but this process was found to be extremely weak due to the small phase space available.

Assuming that the dominant mass defects are isotopes, Fig. 6 shows that, even for a 2.5 mm crystal, a majority of ballistic phonons arriving at the detector have frequencies greater than 230 GHz. (In fact, a good fraction of the transmitted ballistic phonons have frequencies above $\Delta_o/h=325$ GHz.) These phonons have sufficient energy to eject a quasiparticle from a valley, the so-called "exit-valley" events illustrated in Fig. 17(b).

One can see that for narrow valleys there are many more phonon wave vector directions available for exit-valley scattering. For example, [211] valleys with an angular width of 0.25° would subtend only about 1/600 of the Fermi surface, roughly corresponding to the size of the anomalous specific-heat signal reported in Ref. 10. Phonons that eject quasiparticles from a [211] SDW valley would have wave vectors primarily in the {111} planes, resulting in an absorption pattern like that in Fig. 10(a). The flat regions on the second zone of the Fermi surface [Fig. 9(a)] are clearly responsible for the anisotropy in phonon absorption; however, the observed absorption pattern [Fig. 10(b)] is not itself evidence for SDWs.

Because the existence of line nodes or valleys in the superconducting gap could potentially explain the weak temperature dependence of the phonon-absorption lines, we now examine how the magnitude of α obtained from our data using Eq. (13) could decrease with sample length.

Because exit-valley events would far outweigh in-valley events, only ballistic phonons with $h\nu>\Delta_c$ would have significant absorption by quasiparticles. That is, the absorption coefficient α_1 for phonons with energy $h\nu$ less than Δ_c is far less than the absorption coefficient α_2 for phonons with energy greater than Δ_c. We now modify Eq. (12) to have two

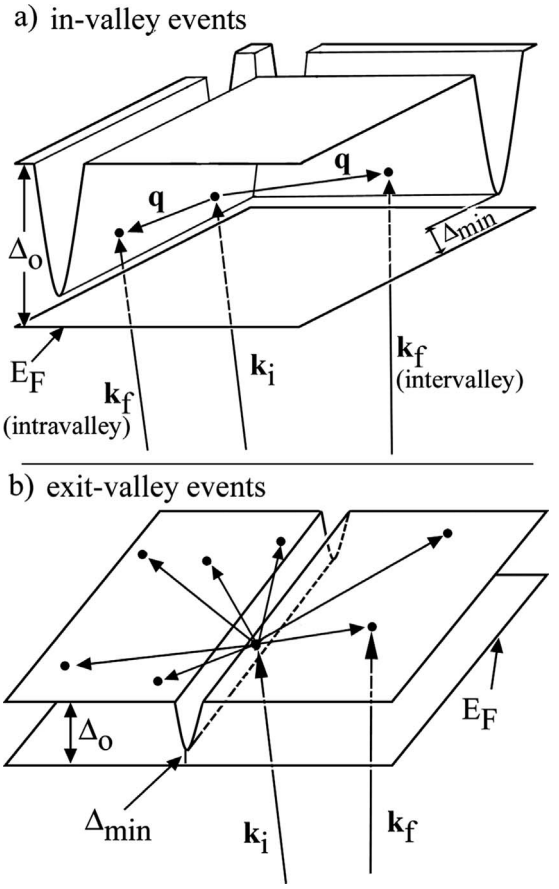

FIG. 17. Diagram of (hypothetical) sharp gap anisotropy in the superconducting energy gap. The bottom of the valleys corresponds to a minimum gap value of $\Delta_{\min}$ with the full gap value Δ_o on the rest of the Fermi surface. (a) In-valley phonons scatter quasiparticles within the gap valleys as shown and (b) exit-valley phonons scatter a quasiparticle from out a valley to a final state anywhere on the Fermi surface.

terms, one with negligible absorption ($\alpha_1=0$),

$$I(x_o)=I_1+I_2\exp(-\alpha_2 L), \tag{15}$$

corresponding to $h\nu<\Delta_c$ and $h\nu>\Delta_c$ events, respectively. Refer to Fig. 18 for an illustration of this case. The fitting parameters are $I_{\rm att}$ and I_o in addition to the Gaussian widths σ_o and σ_a. But now it is $A_2=I_{\rm att}/I_2$ that gives the fraction of absorbed phonons with energies greater than Δ_c. The phonons with energy less than Δ_c have negligible absorption. We wish to compute the absorption coefficient,

$$\alpha_2=(-1/L)\ln(1-A_2)=(-1/L)\ln(1-I_{\rm att}/f_2I_0), \tag{16}$$

where $I_o=I_1+I_2$, and $f_2=I_2/I_o$ is the fraction of transmitted phonons with energies greater than Δ_c in the absence of quasiparticle scattering. The last expression gives α_2 in terms of f_2, and the fitting parameters $I_{\rm att}$ and I_o.

The fraction f_2 cannot be determined from the data. We must rely upon our earlier analysis of isotope scattering in Pb. Figure 7 shows the expected phonon-frequency distributions for the two sample thicknesses used in our experiments, indicating a significant decrease in transmitted phonons with

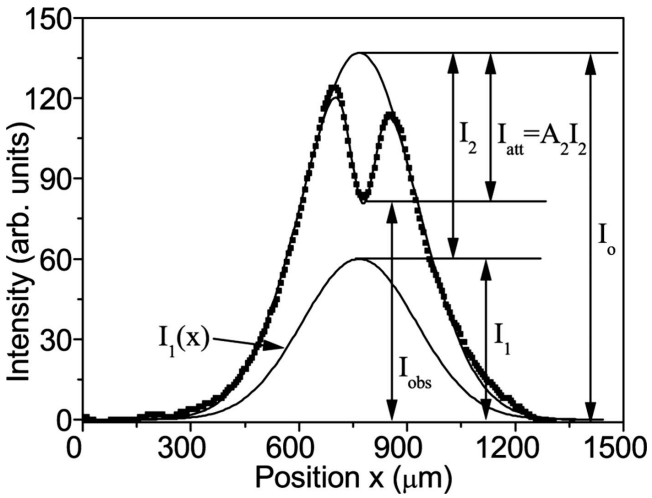

FIG. 18. Graphical description of fitting line scans considering two distributions of phonons. The distribution I_1 is considered as a background signal and I_2 is affected by the absorption along [110].

energies greater than Δ_c as the sample thickness is increased. Figure 19 plots the fractions of LA phonons with energies below the threshold Δ_c for the two sample thicknesses used in our experiments. For example, with $\Delta_{\min}=\Delta_o/3.5$, we obtain the values $f_2 = 0.86$ and 0.76 for the 1 and 2.5 mm crystals, respectively.

In fact, the choice $\Delta_{\min}=\Delta_o/3.5$ is the value of the minimum gap that best collapses the measured values of $\alpha_2(T)$ from the two samples into the same range of absorption at $T\approx 1.8$ K. No single value of $\Delta_{\min}$, however, brings the two data sets into agreement at all temperatures.

Thus, even an allowance for two subsets of ballistic phonons (with energies above and below Δ_c) fails to explain the path-length dependence of absorption. As shown in Fig. 20, separate fits of $\alpha_2(T)$ using the f_2's stated above yield $\Delta_{\min}=\Delta_o/6.3$ and $\Delta_o/2.2$ for 1 and 2.5 mm samples, respectively.

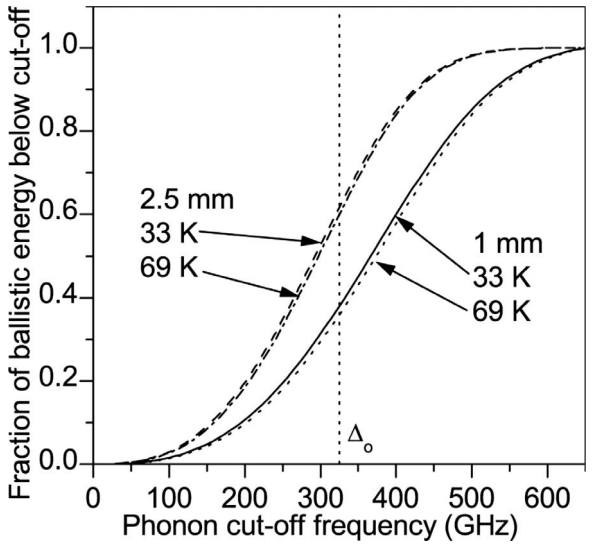

FIG. 19. Fraction of LA phonons f_1 below the cut-off frequency $f_{\text{cut-off}}$ as a function of $f_{\text{cut-off}}$. The parameter f_2, which is the fraction of phonons arriving ballistically at the detector, is defined as $1-f_1$. The ballistic frequency distributions for this calculation are similar to those in Fig. 7. Both 33 and 69 K source temperatures are considered for the 1 and 2.5 mm sample thicknesses.

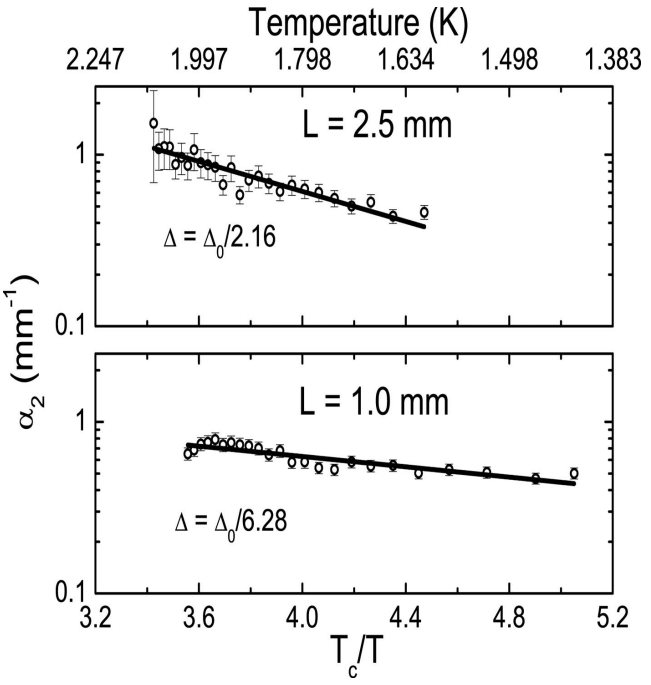

FIG. 20. Phonon absorption coefficient α_2 plotted as a function of T_c/T for 1 and 2.5 mm samples assuming that exit-valley scattering is the dominant process. The magnitudes of α_2 for the two samples are comparable at $T=1.8$ K but the values of Δ_{fit} for the two data sets remain quite different like the data of Fig. 13.

VII. DIRECT TEST OF TWO-COMPONENT ABSORPTION—A LOW-PASS PHONON FILTER

If the principal source of the phonon-absorption lines were ejection of quasiparticles from deep valleys in the superconducting gap, then an obvious test of this hypothesis is to experimentally eliminate ballistic phonons with energies above $\Delta_c=\Delta_o-\Delta_{\min}$. By arguments given in the last section, exit-valley events should greatly dominate in-valley events and the strength of the absorption lines should be greatly reduced by removing high-frequency phonons.

In principle, rejection of phonons above a given frequency can be accomplished by depositing an absorbing or reflecting layer under the detector film. High frequency phonons with energies above Δ_c would still propagate and scatter throughout the crystal but they would be rejected by the filter, preventing their detection. A filter beneath the excitation film, on the other hand, would be ineffective due to the localized hot spot produced by photoexcitation (see Sec. II C).

For cut-off frequencies in the desired 200 GHz range, significant absorption by a single amorphous or superconducting film requires impractically large thicknesses. A multilayer interference filter turns out to be the most effective way to *reflect* high-frequency phonons with submicron thick films. In practice, it took many trials to produce a low-

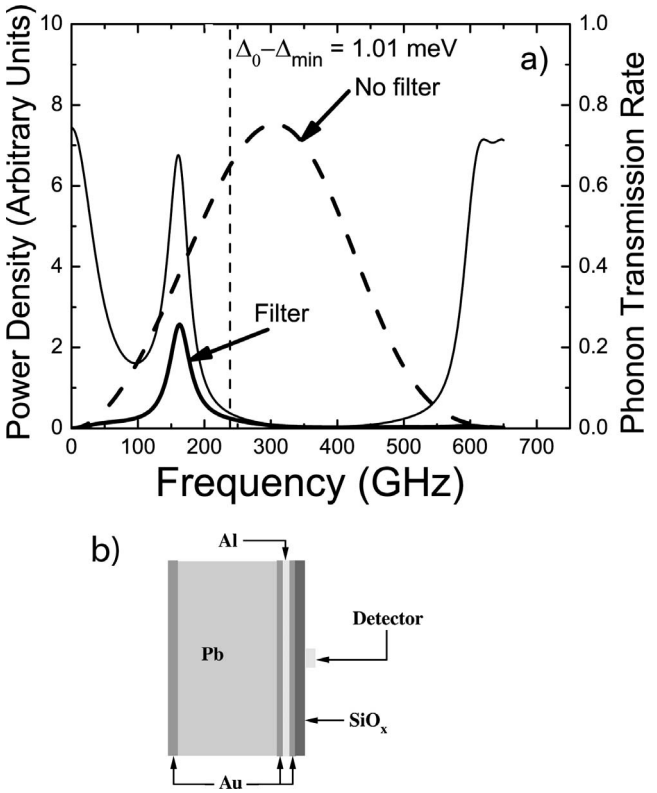

FIG. 21. (a) Transmission function (light solid line) and transmitted power density from a 15 K phonon source through a 1.5 mm Pb sample with (heavy line) and without (heavy dashed line) the low-pass phonon filter. (b) A schematic of the phonon filter experimental configuration. The gold layers on the detection surface are each 100 Å thick, the aluminum layer is 120 Å, the SiO layer is 750 Å, and the detector is 800 Å (Ref. 41). A phonon filter on the excitation side was not feasible due to the localized hot spot produced by photoexcitation.

pass filter on the crystal due to difficulties in coaxing just a few layers with high-contrast impedances to bond to Pb and to each other. In this section, we describe a successful experiment that compares the absorption coefficient for the same sample with and without the phonon filter.

Figure 21(a) shows the calculated transmission of LA phonons for the $Au/Al/Au/SiO_x$ film we fabricated on a 1.6-mm-thick Pb crystal. Part (b) in this figure gives the configuration and dimensions of the films. The 1.6 mm sample with a filter was measured for three points over the temperature range of 1.4–2.1 K. The sample was repolished (thinning it to 1.5 mm), the excitation and detection films were redeposited without a filter, and the experiment was run again. This nonfilter sample was run only at 1.95 K due to limited detector characteristics. As one can see from Fig. 22, the absorption coefficient was found to be nearly the same (within 20%) for filtered and unfiltered cases.[41] Although we have no independent experimental test of the transmittance of the fabricated phonon filter, the straightforward calculation of transmission characteristics and clear experimental result strongly suggest that exit-valley scattering plays little role in the strength of the phonon-absorption lines shown in Figs. 2 and 10.

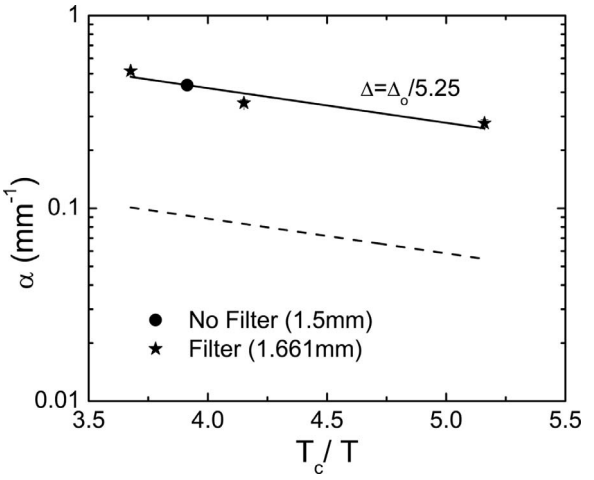

FIG. 22. A plot of α as a function of T_c/T for a 1.6 mm sample including a low-pass phonon filter (stars) and for the same (slightly thinned to 1.5 mm) sample without the filter (dot). The dashed line corresponds to the change in absorption coefficient expected with insertion of the filter if exit-valley scattering is the dominant process. The data with and without the filter fall on the same line, indicating that the exit-valley process is not a major contributor to phonon scattering (Ref. 41).

VIII. SUMMARY AND CONCLUSIONS

Our analysis of the scattering of phonons with quasiparticles on the Fermi surface of Pb explains the highly anisotropic absorption of phonons shown in Figs. 2 and 10(b). Because the second-zone portion of the Fermi surface has large planar regions normal to ⟨111⟩ axes and because the wave vectors of absorbed phonons are directed along the Fermi surface, the absorbed phonons have wave vectors lying in {111} planes.

The absorption of these phonons should depend directly on the number of thermally excited quasiparticles in the superconductor. The phonon absorption indeed increases with increasing temperature; however, the temperature dependence is much slower than expected if the quasiparticles were thermally activated across the accepted gap of Pb, $\Delta_o = 1.35$ meV. The apparent activation energy over our 1.45–2.1 K temperature range is roughly four to six times smaller than Δ_o, depending on crystal thickness.

This puzzle has led us to examine the possibility that the ground state of Pb is associated with spin-density waves (SDWs) that cause deep depressions (or valleys) in the superconducting gap, as proposed by Overhauser and Daemen. We have applied the idea of an SDW to the actual Fermi surface of Pb, using the analysis of Anderson and Gold. A commensurate SDW with wave vector along [211] would have a magnitude very close to $2\mathbf{k}_{Fermi}$ and could lead to absorption of LA phonons with wave vectors in {111} planes. However, in addition to their weak temperature dependences, the measured absorption coefficients for crystals of two thicknesses (1 and 2.5 mm) are significantly different.

For isotope limited phonon scattering (Fig. 6), events in which phonons eject a quasiparticle from an SDW valley (exit-valley events) would far outweigh in-valley scattering

events. If such valleys existed, therefore, the phonon-absorption coefficient would be highly frequency dependent, exhibiting a cutoff at frequencies below a critical phonon energy Δ_c—the depth of a valley. This could explain a path-length dependence of phonon-absorption coefficient.

To address this issue, we have modeled the intensity of the absorption lines assuming that only ballistic phonons with frequencies greater than Δ_c/h can be absorbed by quasiparticles in the valleys. Because high-frequency phonons have less chance of transmission through a thicker sample, the model indeed predicts reduced absorption coefficients for the thicker sample; however, the resulting activation energies for the two samples (1 and 2.5 mm) differ by nearly a factor of three.

To investigate this inconsistency in the exit-valley model, we fabricated a multilayer phonon filter beneath the bolometer in order to reflect phonons with energies $h\nu > \Delta_c$. The strength of the absorption lines was unaffected by this low-pass filter, greatly undermining the case for a highly anisotropic gap in superconducting Pb.

In the following paper, we will consider the role of nonequilibrium phonons, which turns out to be the key to resolving this issue and understanding the scattering of phonons by quasiparticles in Pb.

ACKNOWLEDGMENTS

We thank A. Overhauser for his helpful discussions in the early stages of this work. We are grateful to Matt Hauser for early assistance and paving the way with his experiments on Nb, and we acknowledge helpful interactions with Keith O'Hara and Paul Welander. This work was supported in part by the U.S. Department of Energy under Materials Research Laboratory Grant No. DEFG02-91ER45439.

*Present address: General Electric Global Research Center, Niskayuna, New York 12309, USA.

†Present address: Abilene Christian University Physics Department, Abilene, Texas 79699, USA.

[1] J. R. Anderson and A. V. Gold, Phys. Rev. **139**, A1459 (1965).

[2] V. Narayanamurti, R. C. Dynes, P. Hu, H. Smith, and W. F. Brinkman, Phys. Rev. B **18**, 6041 (1978).

[3] J. P. Wolfe, *Imaging Phonons: Acoustic Wave Propagation in Solids* (Cambridge University Press, Cambridge, England, 1998).

[4] M. R. Hauser, R. Gaitskell, and J. P. Wolfe, Phys. Rev. B **60**, 3072 (1999).

[5] J. D. Short and J. P. Wolfe, Phys. Rev. Lett. **85**, 5198 (2000).

[6] M. Tinkham, *Introduction to Superconductivity* (McGraw-Hill, New York, 1998).

[7] N. W. Ashcroft and N. D. Mermin, *Solid State Physics* (Saunders, Philadelphia, 1976).

[8] More recent tunneling studies show that the gap is actually multivalued and slightly anisotropic. See the beginning of Sec. VI. We quote 1.35 meV as a representative value.

[9] P. H. Keesom and B. J. C. van der Hoeven, Jr., Phys. Lett. **3**, 360 (1963).

[10] B. J. C. van der Hoeven, Jr. and P. Keesom, Phys. Rev. **137**, A103 (1965).

[11] A. W. Overhauser and L. L. Daemen, Phys. Rev. Lett. **61**, 1885 (1988).

[12] L. L. Daemen and A. W. Overhauser, Phys. Rev. B **39**, 6431 (1989), their numerical analysis relies on the specific-heat data of Ref. 10.

[13] Samples are 99.9999% pure Pb grown by Metal Crystals & Oxides, Ltd., United Kingdom. Penetration depth and magnetization measurements indicate transition temperatures of $T_c = 7.19$ K, indicating little effect from impurities.

[14] D. L. Waldorf and G. A. Alers, J. Appl. Phys. **33**, 3266 (1962).

[15] O. Weis, Z. Angew. Phys. **26**, 325 (1969).

[16] See Ref. 3 for a discussion of the time constants that allow for this steady-state assumption and more details on the entire experimental setup.

[17] The Kapitza resistances across the multiple interfaces are accounted for empirically in this model. Detailed application of the acoustic mismatch model gives a similar result for these solid-solid interfaces, as studied by M. Hauser, Ph.D. thesis, University of Illinois, 1995.

[18] J. D. Short, Ph.D. thesis, University of Illinois, 2001.

[19] S. I. Tamura, Phys. Rev. B **31**, 2574 (1985).

[20] Pb has a large concentration of naturally occurring isotopes with atomic masses and abundances given by: 203.973 (1.4%), 205.974 (24.1%), 206.976 (22.1%), and 207.977 (52.4%) for an average mass of 207.2 gm/mol. From Ref. 42.

[21] S. B. Kaplan, C. C. Chi, D. Langenberg, J. J. Chang, S. Jafarey, and D. J. Scalapino, Phys. Rev. B **14**, 4854 (1976).

[22] T.-S. Choy, J. Naset, J. Chen, S. Herschfield, and C. Stanton, Bull. Am. Phys. Soc. **45**(1), 42 (2000).

[23] B. L. Blackford and R. H. March, Phys. Rev. **186**, 397 (1969).

[24] G. I. Lykken, A. L. Geiger, K. S. Dy, and E. N. Mitchell, Phys. Rev. B **4**, 1523 (1971).

[25] A. J. Bennett, Phys. Rev. **140**, A1902 (1965).

[26] P. G. Tomlinson and J. P. Carbotte, Phys. Rev. B **13**, 4738 (1976).

[27] A. Floris, A. Sanna, S. Massidda, and E. K. U. Gross, Phys. Rev. B **75**, 054508 (2007).

[28] Recently, Floris *et al.* (Ref. 27) performed first-principles calculations of the superconducting energy gap of Pb, assuming *s*-wave symmetry. While they were quite successful in explaining the existing tunneling data for Pb, they were unable to reconcile their theory with the specific-heat data of Ref. 10.

[29] L. L. Daemen and A. W. Overhauser, Phys. Rev. B **40**, 129 (1989b).

[30] M. A. Woolf and F. Reif, Phys. Rev. **137**, A557 (1965).

[31] Reference 30 is principally a study of superconductors with magnetic impurities. For all samples, the data show nonvanishing tunneling currents at low voltage, which the authors state as unreliable due to the high impedance of the measuring equipment. Authors of Ref. 29, however, regard that the low-voltage data for the undoped sample provides evidence for SDWs.

[32] N. E. Phillips, M. H. Lambert, and W. R. Gardner, Rev. Mod.

Phys. **36**, 131 (1964).
[33] P. Keesom, Discussion Comment published with Ref. 32.
[34] Although Eq. (7) is derived in the limit of low frequencies, the temperature dependence of the scattering rate is the portion of interest for this paper. Our experimental range of 1.5–2.0 K is a factor of three to five below T_c, implying that the number of quasiparticles is exponentially increasing with temperature ($\Delta_o/kT=8.5$ at 2 K). To see if the exponential dependence of Eq. (7) is reasonable for the phonon frequencies used here, the scattering rate of Eq. (7) is plotted, with good agreement, against the rates predicted by Kaplan *et al.* in Fig. 8(a).
[35] B. R. Tittmann and H. E. Bömmel, Phys. Rev. **151**, 178 (1966).
[36] W. A. Fate, R. W. Shaw, and G. L. Salinger, Phys. Rev. **172**, 413 (1968).
[37] The sample measure in Ref. 36 is deformed by 0.2%. In this sample, they measure a temperature dependence significantly slower than that expected from BCS.
[38] B. R. Tittmann and H. E. Bömmel, Phys. Rev. **151**, 189 (1966b).
[39] The SDW transition temperature predicted by Overhauser to be approximately 600 K, implying that the minimum gap would be constant over our temperature range, where the BCS gap is relatively constant.
[40] For simplicity of notation we will always take **Q** to be along the z axis regardless of the actual crystallographic orientation. The proper orientation of **Q** is considered in all physical simulations.
[41] T. L. Head, Ph.D. thesis, University of Illinois, 2007.
[42] *CRC Handbook of Chemistry and Physics*, edited by D. R. Lide (CRC, Boca Raton, FL, 1991).